Structural Basis of Substrate Selectivity in the Glycerol-3-Phosphate: Phosphate Antiporter GlpT

Christopher J. Law,[†‡] Giray Enkavi,[§¶] Da-Neng Wang,[†‡] and Emad Tajkhorshid[§¶*]

[†]Helen L. and Martin S. Kimmel Center for Biology and Medicine, Skirball Institute of Biomolecular Medicine, and [‡]Department of Cell Biology, New York University School of Medicine, New York, New York; and [§]Department of Biochemistry, Center for Biophysics and Computational Biology, and [¶]Beckman Institute for Advanced Science and Technology, University of Illinois at Urbana-Champaign, Urbana, Illinois

ABSTRACT Major facilitators represent the largest superfamily of secondary active transporter proteins and catalyze the transport of an enormous variety of small solute molecules across biological membranes. However, individual superfamily members, although they may be architecturally similar, exhibit strict specificity toward the substrates they transport. The structural basis of this specificity is poorly understood. A member of the major facilitator superfamily is the glycerol-3-phosphate (G3P) transporter (GlpT) from the *Escherichia coli* inner membrane. GlpT is an antiporter that transports G3P into the cell in exchange for inorganic phosphate (P_i). By combining large-scale molecular-dynamics simulations, mutagenesis, substrate-binding affinity, and transport activity assays on GlpT, we were able to identify key amino acid residues that confer substrate specificity upon this protein. Our studies suggest that only a few amino acid residues that line the transporter lumen act as specificity determinants. Whereas R45, K80, H165, and, to a lesser extent Y38, Y42, and Y76 contribute to recognition of both free P_i and the phosphate moiety of G3P, the residues N162, Y266, and Y393 function in recognition of only the glycerol moiety of G3P. It is the latter interactions that give the transporter a higher affinity to G3P over P_i.

INTRODUCTION

Active transport of solutes across biological membranes is catalyzed by two types of membrane transporter proteins that utilize either the energy released from the hydrolysis of ATP (the primary active transporters) or the energy stored in electrochemical gradients (the secondary active transporters) to drive the transport reaction. One of the largest families of secondary active transporters is the major facilitator superfamily (MFS), currently with 15,000 identified members spread throughout all three kingdoms of life (1–3). Individual representatives of this evolutionarily related family of proteins transport only one or a few related substrates, whereas the MFS as a whole transports an enormous diversity of small polar or charged species, including ions, sugars, organic phosphates, drugs, neurotransmitters, amino acids, and even peptides. But how can individual family members generally display stringent specificity toward the substrates they transport while at the same time the entire family recognizes and transports such a myriad of substrate types? The substrate specificity of each transporter must therefore be defined by only a few amino acid residues and, in particular, by differences between primary sequences at the substrate binding site (4).

Regardless of their diverse substrate specificity, primary sequence analysis suggests that all MFS transporters share a similar structural design that most commonly consists of 12 transmembrane (TM) α-helices separated into six-helix N- and C-terminal domains related by a pseudo twofold symmetry and connected by a long cytoplasmic loop (3). The N- and C-terminal halves of the transporter bestride a central substrate translocation lumen (Fig. 1 *A*). The determination of three-dimensional structures of four prokaryotic representatives of the MFS (5–10) has permitted a better mechanistic understanding of membrane transport (11). Implied from these structures is that MFS transporters function via a single binding-site, alternating access mechanism (12) accompanied by a rocker switch-type movement of the N- and C-terminal domains of the protein (5,6,13), allowing access to the binding site to cycle between the cytoplasm and periplasm. The rocker switch mechanism invokes at least three major conformational states during the transport cycle: a cytoplasmic or inward-facing conformation (C_i), an outward-facing one (C_o), and a more compact, occluded conformation in the transition state (4,13).

Given that the structures of all MFS transporters solved to date are similar, indicating that all the family members are probably architecturally alike, it remains to be determined how each MFS transporter differentiates its cognate substrate from an array of substrates that are often chemically and structurally very similar. Previous descriptions of the basis of substrate selectivity in several transporters have been hampered by a lack of high-resolution structures (14–21). In contrast, studies on the MFS lactose/H^+ symporter LacY, for which high-resolution structural information is available (6,7), have enabled the amino acid residues involved in substrate specificity and binding to be well documented (22–27). Despite this, a detailed description of the structural basis of substrate selectivity is lacking for nearly all other MFS transporters.

Submitted May 29, 2009, and accepted for publication June 30, 2009.

Christopher J. Law and Giray Enkavi contributed equally to this work.

*Correspondence: emad@life.uiuc.edu

Editor: Robert Nakamoto.

0006-3495/09/09/1346/8 $2.00

doi: 10.1016/j.bpj.2009.06.026

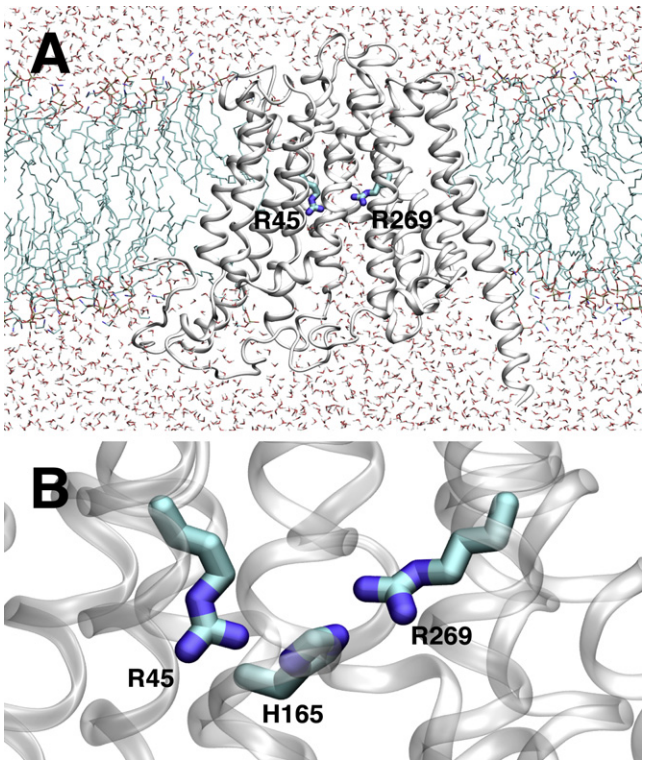

FIGURE 1 Crystal structure of GlpT (Protein Data Bank 1pw4) was used as a starting point for simulations. (*A*) The overall structure of GlpT as viewed along the membrane plane. A section of membrane bilayer and water molecules are also shown to represent the simulation system. (*B*) A close-up view of the substrate binding-site region. The essential arginine residues R45 and R269, and the central histidine H165 are shown explicitly.

The glycerol-3-phosphate (G3P) transporter (GlpT) from the *Escherichia coli* cytoplasmic membrane (28) (Fig. 1) is an MFS antiporter that couples the uptake of G3P, an important precursor for phospholipid biosynthesis, into the cell to the outward movement of inorganic phosphate (P_i) down its concentration gradient (29). GlpT is also of pharmaceutical and medical interest in that it can transport phosphomycin, the only known naturally occurring phosphate-based antibiotic, into the bacterial cell (30,31), and loss-of-function mutations in GlpT result in phosphomycin resistance (32). GlpT is also a homolog of the human endoplasmic reticulum glucose-6-phosphate (G6P) transporter (G6PT) (33), mutations in which cause glycogen storage disease type 1b (GSD-1b) (34,35).

Residues in GlpT that bind to P_i or the phosphate moiety of G3P when the transporter is in the C_i conformation were previously identified to be R45, K80, H165, and R269 (Fig. 1 *B*) (5,36). The affinity of the transporter for G3P is much higher than it is for P_i (13,37), and this discrimination is crucial for the transporter function in that the rate of transport is determined by substrate association/dissociation reactions (4,28). When the substrate-binding site is exposed to the periplasm (the C_o conformation), the much lower affinity of the transporter to P_i allows that substrate to be replaced by G3P. After being transported across the membrane into the cytoplasm, G3P is released and replaced by P_i owing to the much higher intracellular concentration (~4 mM) of the latter (38), thus perpetuating the transport cycle. However, it has not yet been established how GlpT or other antiporters discriminate against and reject noncognate substrates.

We hypothesize that only a few of the residues that line the lumen of GlpT are required to impart discrimination between substrates. To test this hypothesis, we first performed molecular dynamics (MD) simulations to simulate the process of binding of P_i and G3P to GlpT in the C_i conformation, and to probe residues that may be involved in substrate recognition and selectivity. Subsequent biochemical analyses using binding assays of GlpT mutants in detergent solution and transport assays on reconstituted proteoliposomes were used to test the function of each selected residue. This approach has enabled us to offer a description of the structural basis of substrate selectivity in this integral membrane antiporter.

MATERIALS AND METHODS

Modeling of GlpT in membrane

The GlpT structure (5) (Protein Data Bank entry 1pw4) was used as the initial model, in which the mutated residues were reverted back to the wild-type ones, and missing side chains were modeled using the PSFGEN plugin of VMD (39) (Fig. 1). The missing interdomain loop was also modeled, initially as an unstructured chain, and relaxed in vacuum for 100 ps with the rest of the protein fixed. After internal water molecules were added with DOWSER (40), the protein was embedded in a patch of POPE (1-palmytoil-2-oleoyl-*sn*-glycero-3-phosphatidylethanolamine) bilayer with the membrane normal along the z axis. The lipid molecules overlapping with the protein were removed, and the system was solvated and ionized with 100 mM NaCl to produce an electroneutral system. The final dimensions of the system were $115 \times 115 \times 110$ Å^3, including ~125,000 atoms. The system was then subjected to a series of energy minimization and partially constrained MD relaxations before it was freely equilibrated for 5 ns under NP_nT (constant area) conditions. The resulting system (see Fig. 1) was used as a starting point for all subsequent simulations, unless specified otherwise.

Substrate-binding simulations

The substrates (P_i and G3P) were initially placed close to the mouth of the lumen on the cytoplasmic side of GlpT, with the phosphate moieties ~15 Å away from R45 (the putative binding site). After minimization for 5000 steps was completed, each system was simulated for 50 ns to establish stable binding of the substrates and obtain a clear description of the binding site as the substrates explored it. H165 was maintained in an unprotonated state during the simulations. Additionally, GlpT was also simulated in its *apo* form as a control. The W138R mutant was simulated both in the *apo* state and in the presence of either P_i or G3P. Simulations were carried out using a time step of 1 fs, a temperature of 310 K, and a pressure of 1 atm along the z-direction (NP_nT). The simulations were performed with NAMD 2.6 (41) using the CHARMM27 force field with ϕ/ψ cross-term map (CMAP) corrections (42). Water molecules were modeled as TIP3P (43). The force-field parameters for the substrates were adopted from similar molecules in the CHARMM force field. Constant pressure was maintained by the Nosé--Hoover Langevin piston method (44,45), and constant temperature was maintained by Langevin dynamics with a damping coefficient of 1 ps^{-1}

for nonhydrogen atoms. The short-range interaction cutoff was set to 12 Å. Long-range electrostatic interactions were computed using the particle mesh Ewald (PME) method (46) with a grid density of at least 1 $Å^{-3}$. Bonded, nonbonded, and PME calculations were performed using 1, 2, and 4 fs time steps, respectively.

Contact analysis between transporter and substrates

To characterize the interaction between the protein and the substrate, a contact analysis was performed on the 50-ns-long substrate-binding trajectories. All residues with any atom within 3 Å of either the phosphate or the glycerol moiety (in the case of G3P) were considered interacting. The probability of contact between the substrate and the protein was then defined as the ratio of the number of trajectory frames in which a contact existed over the total number of trajectory frames. To filter out transient contacts, only residues exhibiting contact probabilities higher than 25% for the phosphate moiety and 15% for the glycerol moiety are reported.

Bacterial strains, plasmids, and site-directed mutagenesis

GlpT protein used in this study was expressed in *E. coli* LMG194 cells as described before (37). Mutant GlpT transporters were constructed using the QuikChange site-directed mutagenesis kit (Stratagene, Cedar Creek, TX), and mutations were confirmed by sequence analysis of the full-length plasmid DNA. All chemicals were purchased from Sigma Chemicals (St. Louis, MO) unless otherwise stated.

Cell culture, protein purification, and reconstitution of GlpT

Cells were cultured and protein used for substrate binding affinity assays was purified to homogeneity as described previously (37). The protocol for purification of His-tagged GlpT for reconstitution into proteoliposomes has been published before (47). Reconstitution was performed using a modification of the detergent dilution method described previously (36). Lipid stocks were prepared by dissolving 100 mg of *E. coli* polar lipid extract (Avanti Polar Lipids, Alabaster, AL) in 2.5 mL of spectroscopic grade chloroform. The dissolved lipid was split into 5 × 500 μL aliquots in a glass test tube, and each aliquot was dried down on ice under nitrogen stream. To remove all remaining traces of solvent, each tube was placed under vacuum for at least 12 h. Then 2 mL of loading buffer (100 mM potassium phosphate, pH 7.0) were added to each tube to give 2 mL of 10 mg/mL lipid, and the tubes were vortexed thoroughly to resuspend the dried lipid. The lipid mixtures were then snap-frozen in liquid nitrogen before undergoing 10 rounds of freeze (in liquid nitrogen) and thaw (in a 37°C water bath). After the final thaw, the lipid mixture was extruded 13 times through a 400 nm polycarbonate filter (Whatman, Maidstone, England) fitted to a Mini-Extruder (Avanti Polar Lipids) that was preheated to 50°C on a heating block. To make the resulting large unilamellar vesicles (LUVs) "leaky" and ready to incorporate protein, octyl-β-D-glucopyranoside (OG) (Anatrace, Maumee, OH) was added to a final concentration of 1.2% (w/v) and the solution was stirred on ice for 10 min. Purified GlpT was added to the LUVs to obtain a protein/lipid ratio of ~1:150, and the mixture was stirred on ice for an additional 20 min to form proteoliposomes. For a negative control (to measure the "tightness" of the LUVs), protein purification buffer instead of protein was added to an aliquot of LUVs. To seal the proteoliposomes, they were rapidly injected into 50 mL of room temperature (23°C) loading buffer in an ultracentrifuge tube. The proteoliposomes were harvested by centrifugation at 180 k × *g* at 4°C for 1 h. The surfaces of the proteoliposome pellets were washed twice with 2 mL of ice-cold assay buffer (100 mM K_2SO_4, 50 mM MOPS-K, pH 7.0) before they were taken up in the desired volume of the same buffer. The proteoliposomes were kept on ice until used, usually within 2 h of harvesting.

Transport assays

The transport activities of mutant GlpT transporters were assayed over a 10-min period. Freshly prepared P_i-loaded proteoliposomes were taken up in 600 μL of assay buffer (100 mM K_2SO_4, 50 mM MOPS-K, pH 7.0) and 100 μL of this were used for each assay. The proteoliposomes were equilibrated to room temperature (23°C) for 2 min before addition of [^{14}C]-G3P (150 mCi/mmol; American Radiolabeled Chemicals, St. Louis, MO) to 50 μM to initiate transport. At five different time points, 20 μL aliquots of proteoliposomes were removed and applied to 0.22 μm nitrocellulose filters (0.22 μm; Millipore GSWP 02500) mounted on a Hoefer (San Francisco, CA) vacuum manifold. Washing the filter-bound proteoliposomes with two 5 mL aliquots of ice-cold assay buffer terminated the transport reaction. The filters were incubated overnight in liquid scintillant (ScintiLene, Fisher Scientific, Pittsburgh, PA) before the radioactivity was measured with a Wallac 1450 Microbeta Plus liquid scintillation counter.

Substrate binding affinity assays

The affinity of both wild-type and mutant GlpT to free P_i, G3P, and phosphomycin substrates was assayed by measuring the quenching of the intrinsic tryptophan fluorescence of GlpT upon binding of substrate in a detergent solution consisting of 50 mM imidazole, 100 mM NaCl, 0.5 mM EDTA, 20% (w/v) glycerol and 0.075% (w/v) dodecyl maltoside (DDM; Anatrace) at pH 7.0 as described previously (13,36,37). The GlpT protein used for binding studies was purified to apparent homogeneity using size-exclusion chromatography as described by Auer et al. (37). Measurements were performed on a Fluoromax-2 fluorimeter (Jobin-Yvon, Edison, NJ) using a 1 cm × 1 cm quartz cuvette containing 3 mL of a 0.01 mg/mL GlpT solution that was under constant stirring. Slit widths on the fluorimeter were set to 3.0 and 4.5 for excitation and emission, respectively. The cuvette was placed in a water-cooled cuvette holder that was maintained at a temperature of 15°C by a thermostatically controlled water bath. Due to slight differences in the absorption and fluorescence emission maxima between the wild-type and mutant GlpT transporters studied, slightly different fluorescence excitation and emission wavelengths were employed for each protein. The excitation and emission wavelengths were respectively 281 nm and 334 nm for wild-type GlpT, 282 nm and 338 nm for the N162A mutant, and 280 nm and 337 nm for the Y266F and Y393F mutants.

For each experiment, the protein-detergent solution was titrated with either potassium phosphate, *sn*-glycerol 3-phosphate bis(cyclohexylammonium) salt, or the disodium salt of phosphomycin (all made up in the same buffer used for the protein purification) until full fluorescence quenching was observed. After subtraction of the buffer blank and correction for dilution, the fractional fluorescence quenching was plotted as a function of substrate concentration. The data then underwent nonlinear regression analysis using the Enzyme Kinetic Module 1.3 of SigmaPlot 10 (Systat Software, Richmond Point, CA) as described previously (13) to enable calculation of apparent dissociation constant values. Experiments were performed in triplicate.

RESULTS AND DISCUSSION

MD simulations identify amino acid residues that have the potential to function as substrate specificity determinants

To investigate the molecular basis of differences in binding mode and affinity of GlpT for organic and inorganic phosphates, we first studied transporter-substrate interactions by means of MD simulations, an approach that was recently extended to successfully characterize protein-substrate interactions in other membrane transporters (48–50). Using the crystal structure of GlpT in the inward-facing C_i

conformation (5) as the starting point (Fig. 1 *A*), we were able to describe spontaneous binding of the substrates to the transporter without applying any biasing potential or force. These unbiased simulations were performed in the presence of either P_i or G3P initially placed ~15 Å away from R45 in the putative binding site. Both substrates were simulated in their divalent form to exclude complications due to the effect of titration state on the results. The substrates (G3P and P_i) were simulated in both their monovalent and divalent titration states (in different simulations), representing their most prevalent titration states in solution. Although it is not known whether or to what degree the pK_a of the substrates is affected upon entrance into the lumen, the divalent forms of the substrates appear to be more relevant to the transport cycle of GlpT. Therefore, we will focus our discussion mainly on the results obtained for divalent species, noting that the use of monovalent species did not affect our conclusions. The simulations revealed a rapid, spontaneous translocation of the substrates (in both cases) from their initial position at the mouth of the lumen to its apex, where they stayed bound for the remainder of the simulation. The trajectories allowed us to differentiate the protein residues that specifically interact with either substrate from those that contribute to the binding of only one.

The binding trajectories allowed us to quantify and compare the contact patterns of dibasic P_i and G3P with the protein (Fig. 2). Of importance, a direct comparison of the two substrates reveals distinctive steric and electrostatic effects arising from the glycerol moiety of G3P that may play a role in its higher binding affinity. Because GlpT transports both G3P and P_i but not glycerol (37), we hypothesized that interactions between GlpT and the glycerol moiety of G3P hold the key for understanding the protein's substrate specificity. The transporter-substrate interactions can therefore be broken into two main components: the interaction of GlpT with the phosphate moiety based on the data obtained from both the P_i^{2-} and $G3P^{2-}$ simulations, and those involving the glycerol moiety as identified in the $G3P^{2-}$ simulation. During 50-ns simulations, the residues involved in recognition of P_i include the positively charged side chains of R45 and K80 as well as Y38, Y42, Y76, and H165 (Fig. 2 *B*); interactions with Y76, R45, K80, and Y38 occur with the highest frequencies (Fig. 2 *E*). As expected, the interactions involving these residues are mostly electrostatic. The same set of residues contribute to the recognition of both P_i and the phosphate moiety of G3P, although the frequency of substrate contacts for some of these residues (e.g., Y38, K80, and W138) varies from one substrate to another, a difference that is likely due to limited sampling rather than fundamental differences in the binding mode of the phosphate groups in these species. A similar binding mode can be also expected for the phosphate moiety of other small organophosphates, such as phosphomycin. The results indicate that K80, R45, and H165 form the core of the binding site for the phosphate moiety. This is in accord with previous results showing that mutation of K80 or R45 to alanine and lysine, respectively, killed heterologous G3P-P_i transport of the protein reconstituted into proteoliposomes, and mutation of H165 resulted in a transport rate that was only ~6% of that catalyzed by wild-type protein (36).

Although a previously published MD simulation of P_i binding to GlpT (36) showed that the positively charged R269 residue played a role in binding to this substrate, in the work presented here no direct interaction was observed between substrate and R269 over the entire 50-ns duration of any of the simulations. However, since in the earlier work the substrate had already been docked into the lumen of the transporter before the simulation was initiated, the simulation effectively started at a more advanced stage of the binding process. Given that R269 and R45 (Fig. 1 *B*) are both essential residues for GlpT function (mutation of the former to lysine kills GlpT transport activity and decreases the apparent binding affinity of the mutant transporter to substrate G3P by >30-fold, whereas mutation of the latter to lysine abrogates both binding and transport) (36). Mutation of either of the equivalent residues in the closely related *E. coli* homolog sugar phosphate antiporter UhpT also results in abrogation of transport by that protein (51), underlining the vital role of these residues. Our results suggest that R269 does not interact with substrate during the earlier stages of the binding process; rather, it plays an important and as yet not fully understood role during more advanced stages of the substrate binding and transport process, probably by helping to pull together the N- and C-terminal halves of GlpT as the transporter undergoes conformational change involving intrahelix motions (52) and tilts (53), and travels toward the substrate-occluded state (5,36), a state outside the timescale of our current simulations.

There are two observed GlpT-G3P binding modes

Several GlpT residues were found to interact with the glycerol, but not the P_i moiety of G3P. Two binding modes, which keep the GlpT-phosphate interaction invariant but differ in their GlpT-glycerol interaction, were observed and characterized during the 50 ns simulation of G3P binding (Fig. 2, *C* and *D*). The first binding mode is apparent during the first half of the simulation and lasts for ~20 ns. In this mode, the glycerol backbone lies parallel to the plane of the membrane, making hydrophobic contacts with the side chain of Y393, whereas the terminal carbon atom of the glycerol backbone is in contact with the backbone of G389 and L390 (Fig. 2 *C*). The binding is further stabilized by hydrogen bonds (H-bonds) between the hydroxy groups of glycerol and the K80 and Y266 side chains. Here, the backbone of G3P adopts a ring-like structure, in which internal H-bonds between the hydroxy groups and the phosphate moiety of G3P form an arrangement that might be favorable due to lack of sufficient hydration for the hydroxy groups in this region. This conformation, which is somewhat reminiscent of the cyclic structure of phosphomycin (Fig. 2 *A*), is ideal for optimal interaction with Y393. In the second

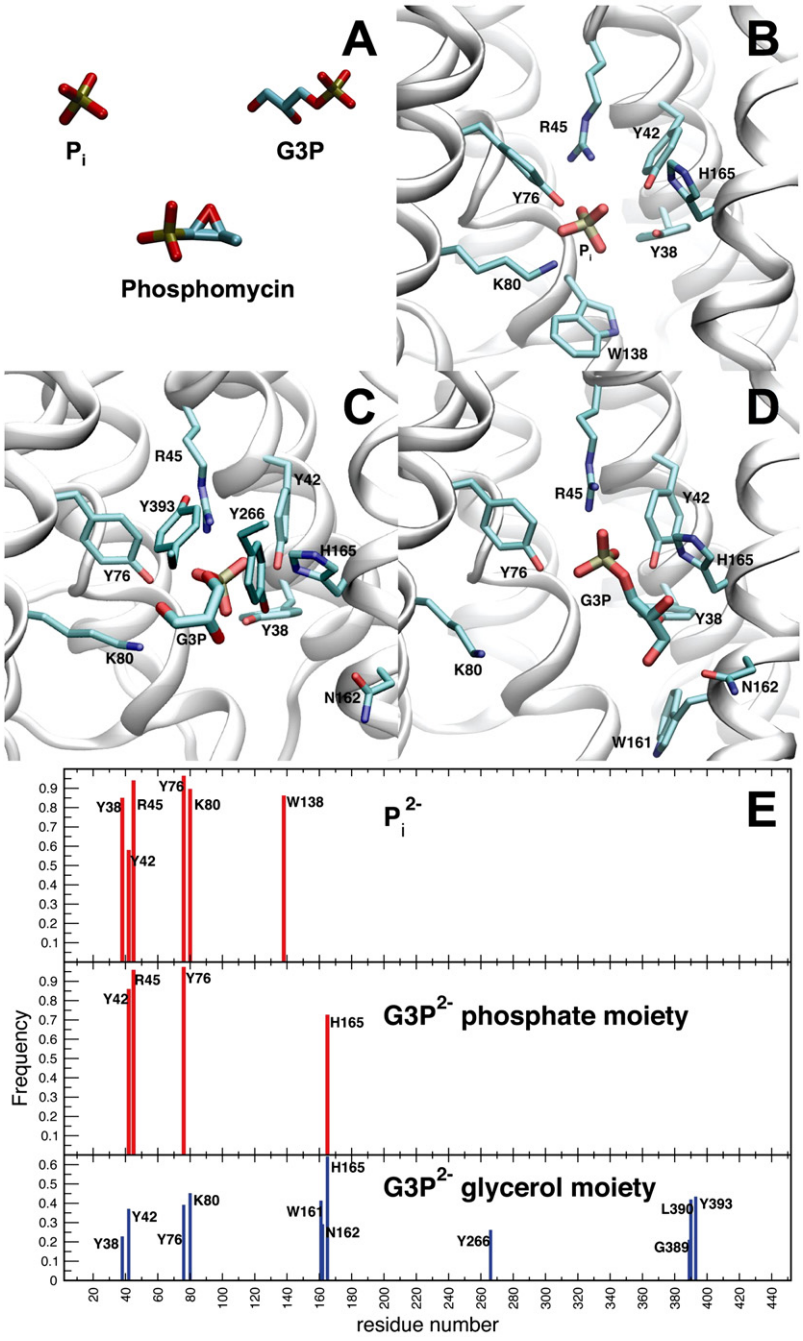

FIGURE 2 Substrate binding in GlpT. (*A*) Molecular structures of GlpT substrates, dibasic phosphate (P_i^{2-}), dibasic glycerol-3-phosphate ($G3P^{2-}$), and phosphomycin. (*B–D*) The protein is rotated ~90° around the *z* axis with respect to the view in Fig. 1 *A* to enable visualization of all the binding-site residues. (*B*) Binding mode of P_i^{2-}. The phosphate group establishes close electrostatic interactions with R45 and K80 while forming H-bonds with Y38, Y42, Y76, and H165. (*C*) First binding mode for G3P. The phosphate moiety of G3P establishes interactions with the GlpT binding site similar to those in the case of P_i. The backbone of G3P forms a ring-like structure (stabilized by intramolecular H-bonds between the hydroxy and phosphate groups) oriented parallel to the plane of the membrane and forms a stacking interaction with Y393, and H-bonds with K80, Y76, and Y266. (*D*) Second binding mode of G3P. The phosphate moiety is in the same location as before and forms the same interactions with the binding pocket. The backbone of G3P is in an extended conformation approximately parallel to the membrane normal, forming H-bonds with N162. (*E*) The results of the contact analysis between the substrate and GlpT (see Materials and Methods). A cutoff distance of 3 Å between any atom from the protein and the substrate is used to define residues that make contact with the substrate. Only residues that maintain contact with the substrate during a fraction $> 25\%$ (for the phosphate groups) and 15% (for the glycerol moiety of G3P) of the duration of the simulation are shown.

binding mode, which is captured during the second half of the simulation and lasts for ~25 ns, G3P adopts a more extended conformation and is no longer parallel to the plane of the membrane (Fig. 2 *D*). It loses interaction with the K80 side chain, but forms contacts with the side chain of H165 as well as H-bonds with N162. There is also a contact between the substrate and the backbone and the C_β atom of W161 in this configuration. Other tyrosine residues (Y38, Y42, and Y76) that line the GlpT lumen also show H-bond interactions with G3P and P_i. Because of its larger size, however, G3P is the only substrate that can also interact, via its glycerol moiety, with the side chains of N162, Y266, and Y393 while bound to R45. Besides the interactions with the GlpT backbone and the residues that also interact with the phosphate moiety of G3P, our simulations suggest a role for the N162, Y266, and Y393 side chains in selecting between P_i and G3P when GlpT is in the C_i conformation.

N162, Y266, and Y393 side chains recognize the G3P glycerol moiety

To confirm that the side chains of N162, Y266, and Y393 are indeed directly involved in binding to the glycerol, but not

the phosphate moiety of G3P, these three residues were mutated to alanine, phenylalanine, and phenylalanine, respectively. We then measured the effects of these GlpT mutations both on the binding affinity of the protein to each substrate in detergent solution and on the G3P-P_i exchange transport activity of each mutant in reconstituted proteoliposomes. The N162A, Y266F, and Y393F mutants bound P_i in detergent solution at neutral pH with apparent K_d values of 4.4 ± 1.4, 1.7 ± 0.4, and 8.6 ± 0.7 μM, respectively (Table 1 and Fig. 3, *B–D*). These values are very similar to the K_d measured for wild-type GlpT binding to P_i, 7.4 ± 0.4 μM (Fig. 3 *A*), thus demonstrating that these residues do not interact with P_i. In stark contrast, and rather surprisingly, none of the above mutants showed any binding to G3P under our assay conditions (Table 1), suggesting that each of these residues plays an important role in the binding and recognition of G3P, particularly its glycerol moiety. It should be noted, however, that our binding assay can only measure K_d values in a concentration range of up to hundreds of micromolars, since above this concentration, complications such as recovery of the fluorescence emission quenching due to secondary effects become apparent. Therefore, it is possible that G3P may bind very weakly to the GlpT N162A, Y266F, and Y393F mutants, but we were not able to detect such a binding. It is also opportune to point out that the K_d values presented here are *apparent* dissociation constants of substrate binding measured in a DDM detergent solution. Under these conditions, a molecule of DDM is bound to the N-terminal half of the lumen of the transporter (36) and must be competed off before the substrate can bind. Also, although the DDM molecule probably stabilizes the inward-facing C_i conformation of the transporter, some of the protein will belong to a population that is in the outward-facing conformation. This means we are measuring a composite of binding to both conformations, but with the major contribution arising from substrate binding to transporter in the inward-facing conformation. We do not yet know whether there is a difference in the binding constants

TABLE 1 Heterologous G3P-P_i exchange transport activity and apparent binding dissociation (K_d) constants of P_i, G3P, and phosphomycin binding to wild-type and mutant GlpT

GlpT protein	K_d P_i binding (μM)	K_d G3P binding (μM)	K_d phosphomycin binding (μM)	G3P-P_i exchange transport activity?
Wild-type	7.4 ± 0.4	0.8 ± 0.2	0.18 ± 0.02	Yes
N162A	4.4 ± 1.4	No binding	No binding	n.d.
Y266F	1.7 ± 0.4	No binding	No binding	No
Y393F	8.6 ± 0.7	No binding	43 ± 6	n.d.

n.d., not determined.

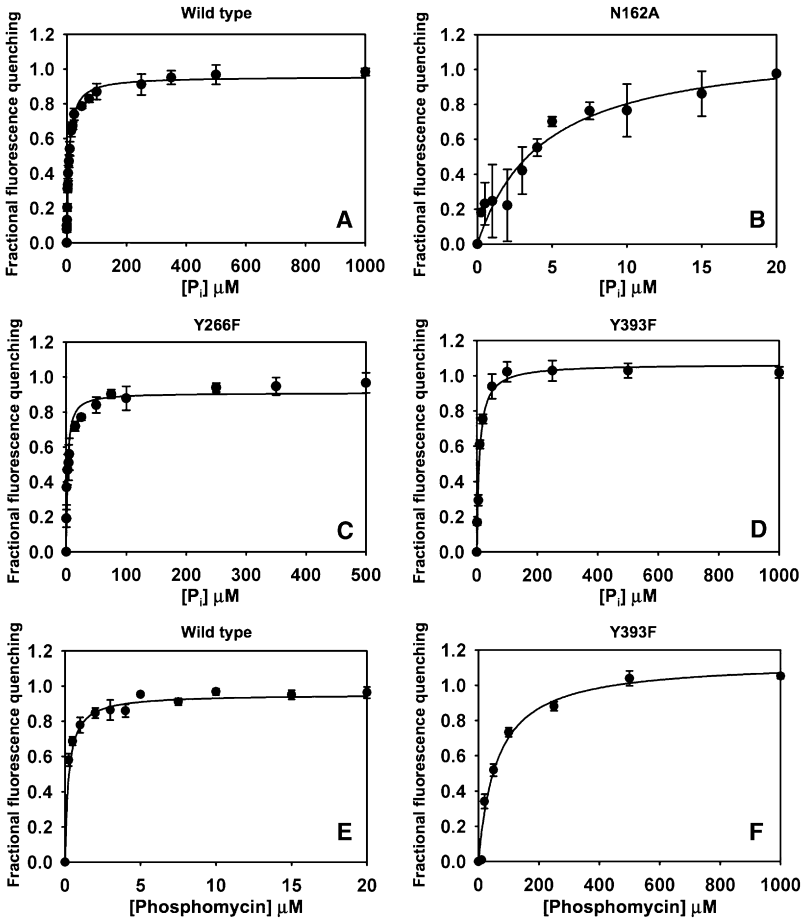

FIGURE 3 Substrate-binding affinity curves showing the fractional intrinsic fluorescence quenching of GlpT as a function of substrate concentration. (*A*) Binding of wild-type GlpT to P_i. (*B*) Binding of GlpT N162A to P_i. (*C*) Binding of GlpT Y266F to P_i. (*D*) Binding of GlpT Y393F to P_i. (*E*) Binding of wild-type GlpT to phosphomycin. (*F*) Binding of GlpT Y393F to phosphomycin. All binding measurements were performed with purified protein in detergent solution. Each data point represents the mean, and error bars represent the mean ± SE of three individual measurements.

for the same substrate in the different transporter conformations, or indeed whether different residues are involved.

No heterologous G3P-P_i exchange transport activity was observed for the Y266F mutant reconstituted into P_i-loaded proteoliposomes (Table 1), a result in accord with the fact that both substrates must be able to bind tightly to the protein for transport to be catalyzed. As a result, transport assays were not performed on the other two mutants. Thus, the binding and transport assays of the site-directed mutants, along with MD simulations, clearly showed that N162, Y266, and Y393 indeed play a role in discriminating between organic and inorganic phosphates.

The fact that mutation of residues associated with either of the two G3P binding modes identified in the simulations results in deleterious effects on substrate binding underlines the relevance of each binding mode. Although the two sets of G3P-interacting residues could represent sites that are sampled by the substrate at various time points during the initial stages of binding, we favor an alternative explanation. Examination of the crystal structure of GlpT (5) shows that these two sets of G3P-interacting residues identified in the simulations are somewhat spatially apart, and thus a small substrate such as G3P is unlikely to simultaneously interact with both sites in the absence of large protein conformational changes. This agrees with the suggestion that G3P binding results in the GlpT N- and C-terminal domains moving closer together to form an occluded state (4,13), with a subsequent spatial convergence of these residues and the formation of a common binding site that allows simultaneous interaction of G3P with the side chains of N162, Y266, and Y393. The apparent loss of binding affinity to G3P upon mutation of these residues at the substrate concentrations tested in our assay suggests that the contribution to binding affinity from these residues is not just additive—the presence of each residue is a requirement for binding of G3P. According to our binding model, any of the residues that interact with a particular substrate are necessary for tight binding of that substrate. Moreover, we suggest that mutation of any of these residues renders the binding site unfavorable for that substrate, possibly by altering the local geometry and properties of the binding site.

GlpT-phosphomycin interactions

Elucidation of the GlpT substrate-specificity determinants derived from the GlpT-G3P and GlpT-P_i interactions immediately suggests that the antibiotic phosphomycin, whose structure can be regarded as intermediate between that of P_i and G3P (Fig. 2 *A*), will interact with some of the same residues (more residues than does P_i, but fewer than G3P). We tested this by performing binding experiments with purified protein in detergent solution. The N162A and Y266F mutants showed no binding to phosphomycin. However, the Y393F mutant did bind the antibiotic with an apparent K_d of 43 $\pm$ 6 μM (Table 1 and Fig. 3 *F*). This is ~240-fold less tight than binding of the wild-type transporter to phosphomycin, which is 0.18 $\pm$ 0.02 μM (Table 1 and Fig. 3 *E*). These studies provide strong support for our prediction that N162 and Y266 play an important role, probably in recognizing the phosphomycin epoxide group as well as the glycerol moiety of G3P.

CONCLUSIONS

The work presented here shows clearly that the structural basis of substrate selectivity in GlpT in the C_i conformation depends on only a handful of residues that line the transporter's lumen. These residues can be divided into three groups: 1), the side chains of R45, Y38, Y42, and Y76 that recognize and bind only P_i and the phosphate moiety of G3P; 2), the K80 and H165 side chains that can interact with both P_i and the glycerol moiety of G3P; and 3), the N162, Y266, and Y393 side chains and the backbones of G389 and L390 that recognize and bind only the glycerol moiety of G3P. Interactions with the second and third groups of residues give G3P a higher affinity than P_i to GlpT. In the outward-facing C_o conformation, some of the residues responsible for the protein's substrate specificity may be different. Given that the transport mechanism is shared between MFS members, we hope that the lessons learned from this study on GlpT can be applied equally to other MFS proteins, which in turn will help us understand the substrate diversity of the entire MFS.

We acknowledge computer time provided by TeraGrid (grant MCA06N060). This work was supported by National Institutes of Health grants R01-GM067887 (to E.T.) and R01-DK053973 (to D.N.W.).

REFERENCES

1. TransportDB. http://www.membranetransport.org/.
2. Saier, Jr., M. H., J. T. Beatty, A. Goffeau, K. T. Harley, W. H. Heijne, et al. 1999. The major facilitator superfamily. *J. Mol. Microbiol. Biotechnol.* 1:257–279.
3. Pao, S. S., I. T. Paulsen, and M. H. Saier. 1998. Major facilitator superfamily. *Microbiol. Mol. Biol. Rev.* 62:1–34.
4. Lemieux, M. J., Y. Huang, and D. N. Wang. 2004. Structural basis of substrate translocation by the *Escherichia coli* glycerol-3-phosphate transporter: a member of the major facilitator superfamily. *Curr. Opin. Struct. Biol.* 14:405–412.
5. Huang, Y., M. J. Lemieux, J. Song, M. Auer, and D. N. Wang. 2003. Structure and mechanism of the glycerol-3-phosphate transporter from *Escherichia coli*. *Science*. 301:616–620.
6. Abramson, J., I. Smirnova, V. Kasho, G. Verner, H. R. Kaback, et al. 2003. Structure and mechanism of the lactose permease of *Escherichia coli*. *Science*. 301:610–615.
7. Guan, L., O. Mirza, G. Verner, S. Iwata, and H. R. Kaback. 2007. Structural determination of wild-type lactose permease. *Proc. Natl. Acad. Sci. USA*. 104:15294–15298.
8. Hirai, T., J. A. Heymann, D. Shi, R. Sarker, P. C. Maloney, et al. 2002. Three-dimensional structure of a bacterial oxalate transporter. *Nat. Struct. Biol.* 9:597–600.
9. Hirai, T., and S. Subramaniam. 2004. Structure and transport mechanism of the bacterial oxalate transporter OxlT. *Biophys. J.* 87:3600–3607.
10. Yin, Y., X. He, P. Szewczyk, T. Nguyen, and G. Chang. 2006. Structure of the multidrug transporter EmrD from *Escherichia coli*. *Science*. 312:741–744.

11. Locher, K. P., R. B. Bass, and D. C. Rees. 2003. Structural biology. Breaching the barrier. *Science*. 301:603–604.
12. Vidavar, G. A. 1966. Inhibition of parallel flux and augmentation of counter flux shown by transport models not involving a mobile carrier. *J. Theor. Biol.* 10:301–306.
13. Law, C. J., Q. Yang, C. Soudant, P. C. Maloney, and D. N. Wang. 2007. Kinetic evidence is consistent with the rocker-switch mechanism of membrane transport by GlpT. *Biochemistry*. 46:12190–12197.
14. Hall, J. A., M. C. Fann, and P. C. Maloney. 1999. Altered substrate selectivity in a mutant of an intrahelical salt bridge in UhpT, the sugar phosphate carrier of *Escherichia coli*. *J. Biol. Chem.* 274:6148–6153.
15. Hall, J. A., and P. C. Maloney. 2001. Transmembrane segment 11 of UhpT, the sugar phosphate carrier of *Escherichia coli*, is an α-helix that carries determinants of substrate selectivity. *J. Biol. Chem.* 276:25107–25113.
16. Hall, J. A., and P. C. Maloney. 2005. Altered oxyanion selectivity in mutants of UhpT, the Pi-linked sugar phosphate carrier of *Escherichia coli*. *J. Biol. Chem.* 280:3376–3381.
17. Arbuckle, M. I., S. Kane, L. M. Porter, M. J. Seatter, and G. W. Gould. 1996. Structure-function analysis of liver-type (GLUT2) and brain-type (GLUT3) glucose transporters: expression of chimeric transporters in *Xenopus* oocytes suggests an important role for putative transmembrane helix 7 in determining substrate selectivity. *Biochemistry*. 35:16519–16527.
18. Colville, C. A., M. J. Seatter, and G. W. Gould. 1993. Analysis of the structural requirements of sugar binding to the liver, brain and insulin-responsive glucose transporters expressed in oocytes. *Biochem. J.* 294:753–760.
19. Colville, C. A., M. J. Seatter, T. J. Jess, G. W. Gould, and H. M. Thomas. 1993. Kinetic-analysis of the liver-type (Glut2) and brain-type (Glut3) glucose transporters in *Xenopus* oocytes–substrate specificities and effects of transport inhibitors. *Biochem. J.* 290:701–706.
20. Seatter, M. J., S. A. De la Rue, L. M. Porter, and G. W. Gould. 1998. QLS motif in transmembrane helix VII of the glucose transporter family interacts with the C-1 position of D-glucose and is involved in substrate selection at the exofacial binding site. *Biochemistry*. 37:1322–1326.
21. Will, A., R. Grassl, J. Erdmenger, T. Caspari, and W. Tanner. 1998. Alteration of substrate affinities and specificities of the *Chlorella* hexose/H^+ symporters by mutations and construction of chimeras. *J. Biol. Chem.* 273:11456–11462.
22. Guan, L., M. Sahin-Toth, and H. R. Kaback. 2002. Changing the lactose permease of *Escherichia coli* into a galactose-specific symporter. *Proc. Natl. Acad. Sci. USA*. 99:6613–6618.
23. Guan, L., and H. R. Kaback. 2004. Binding affinity of lactose permease is not altered by the H^+ electrochemical gradient. *Proc. Natl. Acad. Sci. USA*. 101:12148–12152.
24. Wu, J. H., and H. R. Kaback. 1994. Cysteine 148 in the lactose permease of *Escherichia-coli* is a component of a substrate-binding site. 2. Site-directed fluorescence studies. *Biochemistry*. 33:12166–12171.
25. Naftalin, R. J., N. Green, and P. Cunningham. 2007. Lactose permease H^+-lactose symporter: mechanical switch or Brownian ratchet? *Biophys. J.* 92:3474–3491.
26. Kwaw, I., K. C. Zen, Y. L. Hu, and H. R. Kaback. 2001. Site-directed sulfhydryl labeling of the lactose permease of *Escherichia coli*: helices IV and V that contain the major determinants for substrate binding. *Biochemistry*. 40:10491–10499.
27. Guan, L., and H. R. Kaback. 2006. Lessons from lactose permease. *Annu. Rev. Biophys. Biomol. Struct.* 35:67–91.
28. Law, C. J., P. C. Maloney, and D. N. Wang. 2008. Ins and outs of major facilitator superfamily, antiporters. *Annu. Rev. Microbiol.* 62:289–305.
29. Hayashi, S., J. P. Koch, and E. C. C. Lin. 1964. Active transport of L-α-glycerophosphate in *Escherichia coli*. *J. Biol. Chem.* 239:3098–3105.
30. Silhavy, T. J., I. Hartig-Beecken, and W. Boos. 1976. Periplasmic protein related to the sn-glycerol-3-phosphate transport system of *Escherichia coli*. *J. Bacteriol.* 126:951–958.
31. Nilsson, A. I., O. G. Berg, O. Aspevall, G. Kahlmeter, and D. I. Andersson. 2003. Biological costs and mechanisms of fosfomycin resistance in *Escherichia coli*. *Antimicrob. Agents Chemother*. 47:2850–2858.
32. Kahan, F. M., J. S. Kahan, P. J. Cassidy, and H. Kropp. 1974. Mechanism of action of fosfomycin (phosphonomycin). *Ann. N.Y. Acad. Sci.* 235:364–386.
33. Almqvist, J., Y. Huang, S. Hovmöller, and D. N. Wang. 2004. Homology modeling of the human microsomal glucose-6-phosphate transporter explains the mutations that cause the glycogen storage disease type Ib. *Biochemistry*. 43:9289–9297.
34. Chen, L. Y., C. J. Pan, J. J. Shieh, and J. Y. Chou. 2002. Structure-function analysis of the glucose-6-phosphate transporter deficient in glycogen storage disease type Ib. *Hum. Mol. Genet.* 11:3199–3207.
35. Hiraiwa, H., C. J. Pan, B. Lin, S. W. Moses, and J. Y. Chou. 1999. Inactivation of the glucose 6-phosphate transporter causes glycogen storage disease type 1b. *J. Biol. Chem.* 274:5532–5536.
36. Law, C. J., J. Almqvist, A. Bernstein, R. M. Goetz, Y. F. Huang, et al. 2008. Salt-bridge dynamics control substrate-induced conformational change in the membrane transporter GlpT. *J. Mol. Biol.* 378:828–839.
37. Auer, M., M. J. Kim, M. J. Lemieux, A. Villa, J. M. Song, et al. 2001. High-yield expression and functional analysis of *Escherichia coli* glycerol-3-phosphate transporter. *Biochemistry*. 40:6628–6635.
38. Vink, R., M. R. Bendall, S. J. Simpson, and P. J. Rogers. 1984. Estimation of H^+ to adenosine 5′-triphosphate stoichiometry of *Escherichia coli* ATP synthase using 31P NMR. *Biochemistry*. 23:3667–3675.
39. Humphrey, W., A. Dalke, and K. Schulten. 1996. VMD: visual molecular dynamics. *J. Mol. Graph.* 14:33–38.
40. Zhang, L., and J. Hermans. 1996. Hydrophilicity of cavities in proteins. *Proteins*. 24:433–438.
41. Phillips, J. C., R. Braun, W. Wang, J. Gumbart, E. Tajkhorshid, et al. 2005. Scalable molecular dynamics with NAMD. *J. Comput. Chem.* 26:1781–1802.
42. Mackerell, A. D., M. Feig, and C. L. Brooks. 2004. Extending the treatment of backbone energetics in protein force fields: limitations of gas-phase quantum mechanics in reproducing protein conformational distributions in molecular dynamics simulations. *J. Comput. Chem.* 25:1400–1415.
43. Jorgensen, W. L., J. Chandrasekhar, J. D. Madura, R. W. Impey, and M. L. Klein. 1983. Comparison of simple potential functions for simulating liquid water. *J. Chem. Phys.* 79:926–935.
44. Martyna, G. J., D. J. Tobias, and M. L. Klein. 1994. Constant-pressure molecular-dynamics algorithms. *J. Chem. Phys.* 101:4177–4189.
45. Feller, S. E., Y. H. Zhang, R. W. Pastor, and B. R. Brooks. 1995. Constant-pressure molecular-dynamics simulation—the Langevin Piston method. *J. Chem. Phys.* 103:4613–4621.
46. Darden, T., D. York, and L. Pedersen. 1993. Particle mesh Ewald–an N.Log(N) method for Ewald sums in large systems. *J. Chem. Phys.* 98:10089–10092.
47. Fann, M. C., A. Busch, and P. C. Maloney. 2003. Functional characterization of cysteine residues in GlpT, the glycerol 3-phosphate transporter of *Escherichia coli*. *J. Bacteriol.* 185:3863–3870.
48. Celik, L., B. Schiott, and E. Tajkhorshid. 2008. Substrate binding and formation of an occluded state in the leucine transporter. *Biophys. J.* 94:1600–1612.
49. Huang, Z. J., and E. Tajkhorshid. 2008. Dynamics of the extracellular gate and ion-substrate coupling in the glutamate transporter. *Biophys. J.* 95:2292–2300.
50. Wang, Y., and E. Tajkhorshid. 2008. Electrostatic funneling of substrate in mitochondrial inner membrane carriers. *Proc. Natl. Acad. Sci. USA*. 105:9598–9603.
51. Fann, M., A. H. Davies, A. Varadhachary, T. Kuroda, C. Sevier, et al. 1998. Identification of two essential arginine residues in UhpT, the sugar phosphate antiporter of *Escherichia coli*. *J. Membr. Biol.* 164:187–195.
52. D'Rozario, R., and M. S. P. Sansom. 2008. Helix dynamics in a membrane transport protein: comparative simulations of the glycerol-3-phosphate transporter and its constituent helices. *Mol. Membr. Biol.* 25:571–583.
53. Tsigelny, I. F., J. Greenberg, V. Kouznetsova, and S. K. Nigam. 2008. Modeling of glycerol-3-phosphate transporter suggests a potential 'tilt' mechanism involved in its function. *J. Bioinform. Comput. Biol.* 6:885–904.